Chapter 5
Pizza-peel handling through a sliding nonprehensile manipulation primitive

Alejandro Gutierrez-Giles, Fabio Ruggiero, Vincenzo Lippiello, Bruno Siciliano

Abstract The sliding primitive is a ubiquitous nonprehensile manipulation task, generally performed by mechanical systems represented by underactuated nonlinear models. A literature review of the recent works dealing with this task is first introduced. Then, a particular nonprehensile manipulation task that has arisen in the framework of the RoDyMan project, *i.e.*, a pizza and peel mechanical system, is addressed. A more in-depth study is presented for this system, including modelling, control, and stability analysis. Finally, a discussion on the current achievements and some directions for future work is provided.
This chapter is based on the work presented in [119].

Alejandro Gutierrez-Giles
CECAv-UNAM, Av. Universidad 3000, Ciudad Universitaria, CDMX, CP 04510, Mexico, e-mail: alejandro_giles@cecav.unam.mx

Fabio Ruggiero
CREATE Consortium & University of Naples Federico II, Department of Electrical Engineering and Information Technology, PRISMA Lab, Via Claudio 21, 80125, Naples, Italy, e-mail: fabio.ruggiero@unina.it

Vincenzo Lippiello
CREATE Consortium & University of Naples Federico II, Department of Electrical Engineering and Information Technology, PRISMA Lab, Via Claudio 21, 80125, Naples, Italy, e-mail: vincenzo.lippiello@unina.it

Bruno Siciliano
CREATE Consortium & University of Naples Federico II, Department of Electrical Engineering and Information Technology, PRISMA Lab, Via Claudio 21, 80125, Naples, Italy, e-mail: bruno.siciliano@unina.it

Table 5.1: Main symbols used in this chapter.

Definition	Symbol
Peel (hand) frame	$\mathcal{H}$
Pizza (object) frame	$\mathcal{O}$
Position of the origin of the frame $\mathcal{H}$ in $\mathcal{W}$	$\mathbf{o}_h = \begin{bmatrix} x_h & y_h & z_h \end{bmatrix}^T \in \mathbb{R}^3$
Position of the origin of the frame $\mathcal{O}$ in $\mathcal{H}$	$\mathbf{o}_o^h = \begin{bmatrix} x_o & y_o & z_o \end{bmatrix}^T \in \mathbb{R}^3$
Rotation matrix of $\mathcal{H}$ with respect to $\mathcal{W}$	$\mathbf{R}_h \in SO(3)$
Rotation matrix of $\mathcal{O}$ with respect to $\mathcal{H}$	$\mathbf{R}_o^h \in SO(3)$
Rotation angle of $\mathcal{H}$ with respect to $\mathcal{W}$ around x_h	$\theta \in \mathbb{R}$
Rotation angle of $\mathcal{O}$ with respect to $\mathcal{H}$ around z_o	$\phi \in \mathbb{R}$
Mass of the peel	$m_h > 0$
Mass of the pizza	$m_o > 0$
First row-first column element of the peel's inertia matrix in $\mathcal{H}$	$I_{hx} \in \mathbb{R}$
Inertia matrix of the pizza in $\mathcal{O}$	$\mathbf{I}_o \in \mathbb{R}^{3\times 3}$
First row-first column element of $\mathbf{I}_o$	$I_{ox} \in \mathbb{R}$
Third row-third column element of $\mathbf{I}_o$	$I_{oz} \in \mathbb{R}$
Gravity acceleration	$g = 9.81$ m/s^2
Force applied over the peel along x_h	$u_h \in \mathbb{R}$
Torque applied around the axis x_h	$\tau_h \in \mathbb{R}$
Linear Coulomb friction coefficient between the pizza and the peel	$\mu_o > 0$
Angular Coulomb friction coefficient between the pizza and the peel	$\mu_\phi > 0$
Desired pizza rotation speed	$\dot{\phi}_d \in \mathbb{R}$
Controller gains	$k_i \in \mathbb{R}$, with $i = 1, \ldots, 9$

5.1 Brief introduction

Nonprehensile manipulation through the sliding primitive is a critical control application in the industry, particularly in the so-called *part feeders*. Accordingly, much research has been carried out over the last years in various directions. For example, optimisation in terms of the time required to positioning and orienting a part on a plane is one of the most pursued objectives. Another direction of research deals with the minimum number of actuators/degrees of freedom required to complete a given sliding motion task.

From a theoretical point of view, the specialists have made a great effort to understand the dynamic effects of all the forces that interact during a sliding manipulation task. In particular, it has been noticed that friction, both static and dynamic, plays a fundamental role in this kind of task. Although there are very precise mechanisms in the actuality that can efficiently move a given part to an arbitrary position and orientation in the plane, most of them carry out this task employing open-loop controllers.

The advantages of the feedback control are well-known inside and outside the control community, and thus there are some efforts to incorporate feedback for nonprehensile sliding manipulation. This chapter aims to design

a model-based feedback controller for a specific sliding manipulation task, which consists of an unactuated disk and a 2-DoF manipulator.

First, a review of the current state of research is introduced, related to moving parts through force fields generated by the friction forces arising when two surfaces in contact are in relative motion. Then, a particular application of the sliding primitive in the context of the RoDyMan project is described, *i.e.*, a pizza and peel manipulation system. A mathematical model is developed for this system, which in turn serves as a base for designing the feedback control strategy.

5.2 State of the art

Manipulating objects through a vibrating surface has been a handy application in the industrial context, in particular for *part feeders*. This application has motivated much research in the last decades. From a theoretical point of view, in the late 1990s, the static equilibrium positions and orientations of two-dimensional parts under planar vector fields are investigated in [67], without specifying which mechanism is employed to create these vector fields. On the other hand, the mechanisms to create such vector fields are analysed in [33], where a pixel-wise array is proposed as a universal planar mechanism. In this same work, the authors establish a theoretical tradeoff between mechanical design and motion planning complexities. The universal parts feeders are studied in [34] for non-symmetric parts in the philosophy of minimalist robotics, *i.e.*, the minimal configuration of resources required to solve a given task. Later, a fascinating result is stated in [259]: a horizontal vibrating plate is a universal planar manipulator, including the construction of the proposed mechanism. This mechanism is improved in [260], where the authors are capable of moving a specific part of several over the plate without moving the remaining ones. A variation of the universal planar manipulator, similar to the one developed in [33], is constructed in [100] by employing three orthogonal actuators. All the approaches mentioned above use open-loop controllers.

To the best of the authors' knowledge, one of the first attempts to introduce feedback is presented in [215], where the authors utilise non-smooth analysis and discontinuous control to stabilise an arbitrary position and orientation of the part. Interestingly, in the same article, it is shown that the open-loop controllers are unstable in the orientation coordinate near the static equilibrium points.

In [326], it is noted that the existing universal planar manipulators always generate a force vector field with zero divergence, which is a practical disadvantage. The authors design a universal planar manipulator up to 6 DoFs that can generate force fields with non-zero divergence to solve this problem. This mechanism is employed in [327] in conjunction with a bang-bang control strategy, contrarily to the commonly employed sinusoidal, to generate

movement in the parts towards and away predefined nodal lines. Later, the same authors proposed an optimal controller to generate a twist field that can position and orient a part using their previously designed universal planar manipulator. The effect of both dynamic and static friction on the velocity of the part is studied in [319], where a strategy is proposed to maximise the transport velocity of the sliding parts.

A task-specific mechanism is designed in [130] to translate and rotate a disk to an arbitrary position and orientation. The Neapolitan pizza chefs inspired this mechanism, and the design philosophy is that of minimalist robotics. The authors analyse several configurations for completing the task, arriving at the solution of a two-DoF manipulator. The mechanism and the control strategy are further improved in [131]. The authors also show in [129] that the same strategy can be applied to rotate a deformable disk. Later, the same authors proposed a model of the deformable object in [254]. At the same time, they also find a correlation between the plate frequency and different kinds of motion, *i.e.* sliding, walking, and running. Finally, in [255], the same authors find that a deformable disk rotates faster than a rigid one. The effects of the friction between the plate and the disk are investigated in the same article.

5.3 Pizza-Peel manipulation task

In this section, a dynamic model is first developed based on the Euler-Lagrange equations of motion and some friction properties found in the literature. Then, a feedback control strategy is designed to rotate the pizza. A stability analysis is later presented to show the boundedness of both pizza and peel coordinates and a limit cycle that rotates the pizza at the desired speed. Finally, a numerical simulation is presented to illustrate the validity of the approach.

5.3.1 Dynamic model

Recall the relevant frames as the world frame, $\mathcal{W}$, the frame attached to the peel (hand), $\mathcal{H}$, and the frame attached to the pizza (object), $\mathcal{O}$, as shown in Fig. 5.1. In this chapter, a superscript is used to denote to which frame is the vector or matrix referenced. When referred to $\mathcal{W}$, this superscript is omitted. It is assumed that that the peel is driven by a robotic manipulator. The generalised coordinates for the peel are chosen to be $x_h \in \mathbb{R}$ and $\theta \in \mathbb{R}$. The generalised coordinates for the pizza are chosen as $x_o, y_o, \phi \in \mathbb{R}$. Therefore, the configuration of the system is completely described by the vector

$$\mathbf{q} = \begin{bmatrix} x_h & \theta & x_o & y_o & \phi \end{bmatrix}^T \in \mathbb{R}^5. \tag{5.1}$$

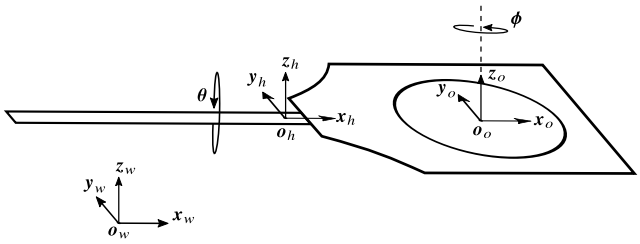

Fig. 5.1: Peel and pizza system.

The pizza centre of mass with respect to $\mathcal{W}$ is given by

$$\mathbf{p}_o = \mathbf{p}_h + \mathbf{R}_h \mathbf{p}_o^h = \begin{bmatrix} x_h + x_o & y_o c_\theta & y_o s_\theta \end{bmatrix}^T , \tag{5.2}$$

where s_x and c_x are shorthand notations for $\sin(x)$ and $\cos(x)$, respectively. The orientation of $\mathcal{O}$ with respect to $\mathcal{W}$ is described by the rotation matrix

$$\mathbf{R}_o = \mathbf{R}_h \mathbf{R}_o^h . \tag{5.3}$$

From this last matrix, one can obtain the pizza angular velocity vector $\boldsymbol{\omega}_o \in \mathbb{R}^3$ through the relation

$$\dot{\mathbf{R}}_o = \mathbf{S}(\boldsymbol{\omega}_o)\mathbf{R}_o \tag{5.4}$$

The kinetic energy, in terms of the generalised coordinates and velocities, is given by

$$\mathcal{T}(\mathbf{q}, \dot{\mathbf{q}}) = \frac{1}{2} m_h \dot{x}_h^2 + \frac{1}{2} I_{hx} \dot{\theta}^2 + \frac{1}{2} m_o \dot{\mathbf{p}}_o^{\mathrm{T}} \dot{\mathbf{p}}_o + \frac{1}{2} \boldsymbol{\omega}_o^T \mathbf{R}_o \mathbf{I}_o \mathbf{R}_o^T \boldsymbol{\omega}_o. \tag{5.5}$$

The potential energy can be computed by

$$\mathcal{U}(\mathbf{q}) = m_o g s_\theta y_o . \tag{5.6}$$

For obtaining the dynamic model, consider the Euler–Lagrange equations of motion

$$\frac{\mathrm{d}}{\mathrm{d}t} \left(\frac{\partial \mathcal{L}}{\partial \dot{\mathbf{q}}} \right)^T - \left(\frac{\partial \mathcal{L}}{\partial \mathbf{q}} \right)^T = \boldsymbol{\xi} \tag{5.7}$$

with Lagrangian $\mathcal{L}(\mathbf{q}, \dot{\mathbf{q}}) = \mathcal{T}(\mathbf{q}, \dot{\mathbf{q}}) - \mathcal{U}(\mathbf{q})$ and the non-conservative and external forces are represented by the vector

$$\boldsymbol{\xi} = \begin{bmatrix} u_h & \tau_\theta & f_x & f_y & \tau_\phi \end{bmatrix}^T , \tag{5.8}$$

where f_x, f_y, and τ_ϕ are explained below.

The Coulomb friction terms play an important role for this particular task. These terms are defined as functions of the relative velocities between the peel and the pizza $\dot{x}_o$ and $\dot{y}_o$, and are described by [131]

$$f_{\mathrm{x}} = m_o g \mu_o \mathrm{sign}(\dot{x}_o) \tag{5.9}$$

$$f_{\mathrm{y}} = m_o g \mu_o \mathrm{sign}(\dot{y}_o)\,, \tag{5.10}$$

where $\mathrm{sign}(x)$ is the function defined by

$$\mathrm{sign}(x) = \begin{cases} 1 & \text{if } x > 0 \\ 0 & \text{if } x = 0 \\ -1 & \text{if } x < 0 \end{cases} .$$

As explained in [131], there is a torque over the $\mathbf{z}_o^h$ axis produced by the movement of the x_h coordinate and the change of the pressure distribution which in turn is induced by the acceleration on the θ coordinate and is given by

$$\tau_\phi = \mu_\phi I_{ox} \mathrm{sign}(\dot{x}_o)\ddot{\theta}. \tag{5.11}$$

By Newton's third law of motion, there must be a reaction torque acting on the θ coordinate. However, this torque can be neglected by assuming that the inertia of the peel is much bigger than that of the pizza.

A further simplification can be made if the linear and angular accelerations of the peel are assumed to be the inputs, *i.e.*,

$$\mathbf{u} \triangleq \begin{bmatrix} u_h & u_\theta \end{bmatrix}^T \triangleq \begin{bmatrix} \ddot{x}_h & \ddot{\theta} \end{bmatrix}^T . \tag{5.12}$$

The following approximation of the sign function is made in order to employ continuous tools to analyse the system dynamics

$$\mathrm{sign}(x_i) \approx \tanh(k_i x_i)\,, \tag{5.13}$$

where each $k_i > 0$ is a constant. The objective is to control the pizza rotation speed, for which the regulation error is defined as

$$\tilde{\dot{\phi}} = \dot{\phi} - \dot{\phi}_d \in \mathbb{R}\,, \tag{5.14}$$

Next, let the state space vector $\mathbf{x} \in \mathbb{R}^9$ be defined by

$$\begin{aligned} \mathbf{x} &= \begin{bmatrix} x_1 & x_2 & \cdots & x_9 \end{bmatrix}^T \\ &\triangleq \begin{bmatrix} x_h & \theta_h & x_o & y_o & \dot{x}_h & \dot{\theta}_h & \dot{x}_o & \dot{y}_o & \tilde{\dot{\phi}} \end{bmatrix}^T . \end{aligned} \tag{5.15}$$

Thus, the system dynamics can be put in the form

$$\dot{\mathbf{x}} = \mathbf{f}(\mathbf{x}) + \mathbf{g}_1 u_1 + \mathbf{g}_2(\mathbf{x}) u_2 \,, \tag{5.16}$$

where

$$\mathbf{f}(\mathbf{x}) = \begin{bmatrix} x_5 \\ x_6 \\ x_7 \\ x_8 \\ \mathbf{f}_2(\mathbf{x}) \end{bmatrix} \qquad \mathbf{g}_1 = \begin{bmatrix} \mathbf{0}_4 \\ \mathbf{g}_{12} \end{bmatrix} \qquad \mathbf{g}_2(\mathbf{x}) = \begin{bmatrix} \mathbf{0}_4 \\ \mathbf{g}_{22}(\mathbf{x}) \end{bmatrix} \,, \tag{5.17}$$

with

$$\mathbf{f}_2(\mathbf{x}) = \begin{bmatrix} 0 \\ 0 \\ -\frac{b_o}{m_o} x_7 - g\mu_o \tanh(k_7 x_7) \\ -\frac{b_o}{m_o} x_8 - g\mu_o \tanh(k_8 x_8) - g\sin(x_2) + x_4 x_6^2 \\ 0 \end{bmatrix} \tag{5.18}$$

$$\mathbf{g}_{12} = \begin{bmatrix} 1 & 0 & -1 & 0 & 0 \end{bmatrix}^T \tag{5.19}$$

$$\mathbf{g}_{22}(\mathbf{x}) = \begin{bmatrix} 0 & 1 & 0 & 0 & -\mu_\phi \left(I_{ox}/I_{oz}\right) \tanh(k_7 x_7) \end{bmatrix}^T . \tag{5.20}$$

By computing the Philip Hall basis [216, p. 344] with the vector fields $\mathbf{f}$, $\mathbf{g}_1$, and $\mathbf{g}_2$, it can be verified that the *accessibility distribution* is of dimension 9 in the set $\mathcal{D} = \left\{ \mathbf{x} \in \mathbb{R}^9 : \dot{\theta} \neq 0, \dot{x}_\mathrm{o} \neq 0, y_\mathrm{o} \neq 0 \right\}$, and therefore the system is *accessible*. Furthermore, by computing the base

$$\{\mathbf{g}_1, \mathbf{g}_2, [\mathbf{g}_1, \mathbf{f}], [\mathbf{g}_2, \mathbf{f}], [\mathbf{g}_1, \mathbf{g}_2], [\mathbf{f}, [\mathbf{g}_1, \mathbf{f},]], [\mathbf{f}, [\mathbf{g}_2, \mathbf{f}]], [\mathbf{f}, [\mathbf{g}_1, \mathbf{g}_2]], [\mathbf{g}_1, [\mathbf{g}_1, \mathbf{f}]], [\mathbf{g}_2, [\mathbf{g}_2, \mathbf{f}]]\}$$

it can be proven that the system is *strongly accessible* in $\mathcal{D}$ [31, p. 180]. Nevertheless, if the centripetal force term $x_4 x_6^2$ is neglected, as it is commonly assumed in the related literature (see for example [328, 131]), the strong accessibility condition is no longer fulfilled, but only the accessibility one, restricted to $\mathcal{D}_\mathrm{a} = \left\{ \mathbf{x} \in \mathbb{R}^9 : \dot{x}_\mathrm{o} \neq 0, \dot{y}_\mathrm{o} \neq 0 \right\}$. The following assumption is made in this work.

Assumption 5.3.1 The centrifugal force term $x_4 x_6^2$ in (5.16) can be neglected. □

This assumption is made to simplify the controller design and the stability analysis, but the term $x_4 x_6^2$ is kept for the numerical simulation of the system dynamics.

5.3.2 Controller design and stability analysis

The control objective of this work is to induce a rotating movement on the pizza dough at a desired angular speed $\dot{\phi}_d$ while keeping the remaining coordinates as close to zero as possible. The contribution of this work is the design of a closed-loop control law for achieving the task mentioned above. The first control law, intended for the linear motion of the peel, is composed of a feedforward term, very similar to the reported open-loop controllers in the literature, plus a PD control to stabilise the linear peel direction, that is

$$u_1 = -k_1 x_1 - k_5 x_5 + a_h \sin(\omega_h t) \tag{5.21}$$

$$u_2 = \frac{\tanh(k_7 x_7) I_{oz}}{\mu_\phi I_{ox}} k_9 x_9 - k_2 x_2 - k_6 x_6 \,, \tag{5.22}$$

with $a_h \in \mathbb{R}$ and $\omega_h > 0$. The feedforward term $a_h \sin(\omega_h t)$ ensures the required condition $\dot{x}_o \neq 0$. On the other hand, the control law (5.22) is a PD control that stabilises the peel orientation, plus a nonlinear term employed to induce a rotation in the pizza by exploiting the torque generated from (5.11).

In order to carry out a mathematical analysis, consider the closed-loop dynamics

$$\begin{aligned}
\dot{x}_1 =& x_5, \\
\dot{x}_2 =& x_6, \\
\dot{x}_3 =& x_7, \\
\dot{x}_4 =& x_8, \\
\dot{x}_5 =& -k_1 x_1 - k_5 x_5 + a_h \sin(\omega_h t)\,, \\
\dot{x}_6 =& -k_2 x_2 - k_6 x_6 + \frac{I_{oz}}{\mu_\phi I_{ox}} \tanh(k_7 x_7) k_9 x_9, \\
\dot{x}_7 =& -g\mu_o \tanh(k_7 x_7) + k_1 x_1 + k_5 x_5 - a_h \sin(\omega_h t)\,, \\
\dot{x}_8 =& -g\mu_o \tanh(k_8 x_8) - g \sin(x_2), \\
\dot{x}_9 =& -k_9 x_9 \tanh^2(k_7 x_7) + \frac{\mu_\phi I_{ox}}{I_{oz}} \tanh(k_7 x_7)\,(k_2 x_2 + k_6 x_6)\,.
\end{aligned} \tag{5.23}$$

The following analysis is developed considering that stationary state has reached. For a more straightforward exposition of the following development, the closed-loop dynamics is divided into the four subsystems shown in Fig. 5.2.

1) The subsystem Σ_1, comprised of the states x_1 and x_5, is a linear stable system with arbitrarily chosen poles by means of the gains k_1 and k_5, under the effect of the sinusoidal input $a_\mathrm{h} \sin(\omega_\mathrm{h} t)$. The amplitude of the states x_1 and x_5 in stationary state are sinusoidals with frequency ω_h and amplitude easily computed to be

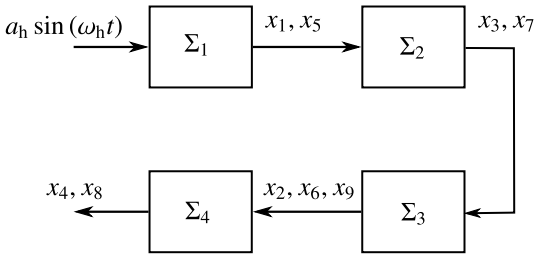

Fig. 5.2: Closed-loop dynamics.

$$|x_1| = \frac{a_h}{D(k_1, k_5, \omega_\mathrm{h})} \tag{5.24}$$

$$|x_5| = \frac{a_\mathrm{h}\omega_h}{D(k_1, k_5, \omega_h)}\,, \tag{5.25}$$

where

$$D(k_1, k_5, \omega_\mathrm{h}) = \sqrt{(k_1 - \omega_h^2)^2 + k_5^2\omega_\mathrm{h}^2}\,. \tag{5.26}$$

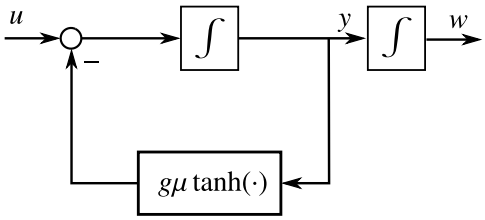

Fig. 5.3: Nonlinear feedback loop.

2) The second subsystem, which corresponds to the states x_3 and x_7, is analysed by employing the *describing function* method [286, p. 157], for which the configuration shown in Fig. 5.3 is considered with $u = -u_1$ and $y = x_7$. To approximate the nonlinearity in the Σ_2 subsystem, the following describing function is used

$$g\mu_\mathrm{o} \tanh(\cdot) \approx \frac{4g\mu_\mathrm{o}}{\pi A(\cdot)}\,, \tag{5.27}$$

where $A(\cdot)$ is the input amplitude of the nonlinear block signal, which in turn is assumed to be sinusoidal. The approximate closed-loop transfer function of the subsystem Σ_2 is

$$y(s) = \left(\frac{\pi A(\cdot)}{s\pi A(\cdot) + 4g\mu_o} \right) u(s) = h(s)u(s)\,. \tag{5.28}$$

The output of this system is the sum of a self-oscillatory response and a forced response [35, Ch. 3]. The frequency of the self oscillatory component ω_{s} is obtained by solving the equation

$$j\omega_{\mathrm{s}} = \frac{4g\mu_o}{\pi A(\cdot)}\,. \tag{5.29}$$

Because $A(\cdot)$ is a positive and real function, no unforced periodic response is present. On the other hand, the gain for the closed-loop pseudo-transfer function can be computed as

$$|h(s)| = \frac{\pi^2 A^2(\cdot)}{\sqrt{\omega_h^2 \pi^2 A^2(\cdot) + 16 g^2 \mu_o^2}}\,, \tag{5.30}$$

which has a minimum at zero and a maximum at ω_h^{-1}. The input to this subsystem is $u = -u_1$, which is a sinusoidal signal with zero mean, frequency ω_h and amplitude bounded by

$$|u_1| \leq \frac{a_h \omega_h^2}{D(k_1, k_5, \omega_h)}\,. \tag{5.31}$$

Therefore, the approximate steady state output of this subsystem is a sinusoidal with zero mean given by

$$x_7 = a_7 \sin\left(\omega_h t + \phi_7\right)\,, \tag{5.32}$$

where

$$|a_7| \leq \frac{a_h \omega_h}{D(k_1, k_5, \omega_h)} \tag{5.33}$$

and $\phi_7 \in \mathbb{R}$ is the phase shift given by

$$\phi_7 = \mathrm{atan2}(-a_h \omega_h, 4g\mu_o/(\pi A(\cdot)))\,, \tag{5.34}$$

which can be bounded by $-\pi/2 \leq \phi_7 \leq 0$. The response in steady state for x_3 can be approximated by

$$x_3 = a_3 \sin\left(\omega_h t + \phi_3\right) + c_3\,, \tag{5.35}$$

where $c_3 \in \mathbb{R}$ is a bias constant, $\phi_3 \in \mathbb{R}$ is a phase shift, and

$$|a_3| \leq \frac{a_{\mathrm{h}}}{D(k_1, k_5, \omega_h)}\,. \tag{5.36}$$

3) For showing the stability properties of the subsystem Σ_3, it is first recalled the following [152, Theorem 10.3].

Theorem 5.3.1

Consider the system

$$\dot{\mathbf{x}} = \mathbf{f}(\mathbf{x}) + \epsilon \mathbf{g}(t, \mathbf{x}, \epsilon)\,. \tag{5.37}$$

Suppose

- $\mathbf{f}$, $\mathbf{g}$, and their first partial derivatives with respect to $\mathbf{x}$ are continuous and bounded for all $(t, \mathbf{x}, \epsilon) \in [0, \infty) \times D_0 \times [-\epsilon_0, \epsilon_0]$, for every compact set $D_0 \subset D$, where $D \subset \mathbb{R}^n$ is a domain that contains the origin.
- The origin is an exponentially stable equilibrium point of the autonomous system

$$\dot{\mathbf{x}} = \mathbf{f}(\mathbf{x})\,; \tag{5.38}$$

- $\mathbf{g}(t, \mathbf{x}, \epsilon)$ is T-periodic in t.

Then, there exist positive constants ϵ^* and k such that for all $|\epsilon| < \epsilon^*$, equation (5.37) has a unique T-periodic solution $\bar{\mathbf{x}}(t, \epsilon)$ with the property that $\|\bar{\mathbf{x}}(t, \epsilon)\| \leq k|\epsilon|$. Moreover, this solution is exponentially stable. □

After employing the identity $\tanh^2(x) = 1 - \mathrm{sech}^2(x)$, the dynamics of the subsystem Σ_3 can be written as equation (5.37) with $\mathbf{x} = \begin{bmatrix} x_2 & x_6 & x_9 \end{bmatrix}^T$ and

$$\mathbf{f} = \begin{bmatrix} x_6 \\ -k_2 x_2 - k_6 x_6 \\ -k_9 x_9 \end{bmatrix} \tag{5.39}$$

$$\mathbf{g} = \begin{bmatrix} 0 \\ \dfrac{1}{c_\mu} \tanh(k_7 x_7) k_9 x_9 \\ \mathrm{sech}^2(k_7 x_7) k_9 x_9 + c_\mu \tanh(k_7 x_7)\,(k_2 x_2 + k_6 x_6) \end{bmatrix} \tag{5.40}$$

where $c_\mu = \mu_\phi I_{\mathrm{ox}} I_{\mathrm{oz}}^{-1}$, $\mathbf{f}(\mathbf{x}) = \mathbf{f}$ and $\mathbf{g}(t, \mathbf{x}, \epsilon) = \mathbf{g}$, with $\epsilon = 1$. As proven in the item 2), the steady state solution for x_7 is a T-periodic function of time t with period $T = 2\pi/\omega_{\mathrm{h}}$, and thus it is $\mathbf{g}$ in (5.40). It is not difficult to prove that the autonomous subsystem $\dot{\mathbf{x}} = \mathbf{f}(\mathbf{x})$, with $\mathbf{f}(\mathbf{x})$ defined in (5.39), is exponentially stable. By applying Theorem 5.3.1 restricted to the region $\mathbb{D} \triangleq \{\mathbf{x} : \|\mathbf{x}\| \leq \rho\}$, with $\rho > 0$, one can conclude that the solution trajectories for the states $\mathbf{x} = \begin{bmatrix} x_2 & x_6 & x_9 \end{bmatrix}^T$ are T-periodic functions of time, and the states converge exponentially to these solutions. As stated in Theorem 5.3.1, the periodic solution is bounded by $\|\bar{\mathbf{x}}(t, \epsilon)\| \leq k|\epsilon|$. Furthermore, from the theory of linear bounded input-bounded output systems, the ultimate bound $k|\epsilon|$ can be made arbitrarily small by making the gains k_2, k_6, and k_9 arbitrarily large.

4) For the fourth subsystem, consider again the block diagram depicted in Fig. 5.3, with $u = g\sin(x_2)$, $y = x_8$, and $w = x_4$. The transfer function employed to approximate this system is given by (5.28). By the same arguments as the given in the item 2), the solution trajectories for this

system can be approximated by

$$x_4 = a_4 \sin(\omega_h t + \phi_4) + c_4 \tag{5.41}$$

$$x_8 = a_8 \sin(\omega_h t + \phi_8)\,, \tag{5.42}$$

where $c_4 \in \mathbb{R}$ is a bias constant and

$$a_4 \leq \frac{c_8 g}{\omega_h^2} \tag{5.43}$$

$$a_8 \leq \frac{c_8 g}{\omega_h}\,, \tag{5.44}$$

with $c_8 = \sup_t(|\sin(x_2(t))|)$.

In summary, the above analysis shows that the approximate solutions of the closed-loop system are bounded and periodic. Furthermore, the ultimate bound for the states x_2, x_6, and x_9 can be driven arbitrarily close to zero, which means that the peel will be as close as desired to the horizontal position and that the pizza rotation speed will be arbitrarily close to the desired value, *i.e.* $\dot{\phi} \approx \dot{\phi}_d$.

5.3.3 Numerical simulation

A numerical simulation is proposed to validate the results of Section 5.3.1. The centrifugal term $x_4 x_6^2$ in (5.20) is kept for the simulation to test the robustness of the controller design. The parameters considered for the system are displayed in Table 5.2.

Table 5.2: Parameters for the numerical simulation.

Meaning	Parameter	Value
Pizza mass	m_o	$0.25\,\mathrm{kg}$
Pizza x-inertia moment	I_ox	$0.01\,\mathrm{kg\,m^2}$
Pizza z-inertia moment	I_oz	$0.028\,\mathrm{kg\,m^2}$
Linear Coulomb friction coefficient	μ_o	0.5
Rotational Coulomb friction coefficient	μ_ϕ	0.5
Gravity acceleration constant	g	$9.81\,\mathrm{m/s^2}$

The parameters of the controller (5.21)–(5.22) were chosen empirically as $\omega_\mathrm{h} = 18\,\mathrm{rad/s}$, $a_\mathrm{h} = 2$, $k_1 = 10$, $k_2 = 10$, $k_5 = 10$, $k_6 = 50$, $k_7 = 20$, and $k_9 = 40$. It is considered that the sample time for the control loop is $T = 5\,\mathrm{ms}$. The desired speed for the pizza rotation is $1\,\mathrm{rad/s}$ in counter-clockwise direction.

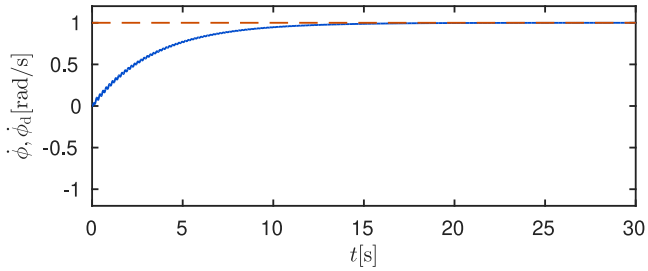

Fig. 5.4: Pizza rotation speed: real (—), desired (- - -)

The actual and desired rotation speed are shown in Fig. 5.4. It can be appreciated that the actual speed is very close to the desired one in the steady-state.

The phase portrait of x_{h} is shown in Fig. 5.5. In this plot and the following ones, a blue marker indicates the initial point, a green line denotes the first 15 seconds (transient response), and a red line indicates the last 15 seconds (steady-state). It can be appreciated that the x_{h} and $\dot{x}_{\mathrm{h}}$ coordinates keep oscillating around zero. Indeed, the amplitude of x_{h} coincides with the one predicted by (5.24), *i.e* , $|x_h|= 5.5 \cdot 10^{-3}$ m. On the other hand, the phase portrait for the θ_{h} coordinate is shown in Fig. 5.6. In this figure, it can be appreciated that in the stationary state, this coordinate remains oscillating very close to zero, following the stability analysis of Section 5.3.1.

The phase portrait for the x_{p} coordinate is shown in Fig. 5.7. The predicted value for the amplitude of the oscillations for x_{p} computed in (5.36) has as an upper bound $|a_3| \leq 5.5 \cdot 10^{-3}$, which is a very conservative one, as can be seen in the figure. The reason behind this large margin is because we are taking the worst case for the pseudo-transfer function gain in (5.30). Finally, the phase portrait for the y_{p} coordinate is displayed in Fig. 5.8. As it can be appreciated in the figure, the oscillation amplitude of this coordinate can be made arbitrarily small, as it depends on the amplitude of θ_{h}, which in turn can be made arbitrarily small. However, in this case, there is a non-negligible bias term of about $6 \cdot 10^{-3}$ m as stated in (5.41).

5.4 Discussion and conclusion

In this chapter, an overview of the sliding manipulation primitive is first given, and then a particular case was studied. The main intention was to underline the potential of moving parts using sliding and the complication arising in the control design and mathematical analysis. The literature review showed that although within the nonprehensile manipulation tasks, the sliding primitive is

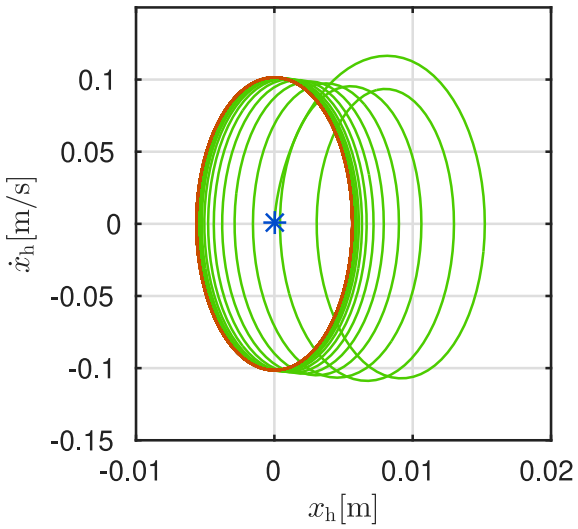

Fig. 5.5: Phase portrait of x_h and $\dot{x}_\mathrm{h}$: $t = 0\,\mathrm{s}$ (∗), $0 < t \leq 15\,\mathrm{s}$ (—), $t > 15\,\mathrm{s}$ (—).

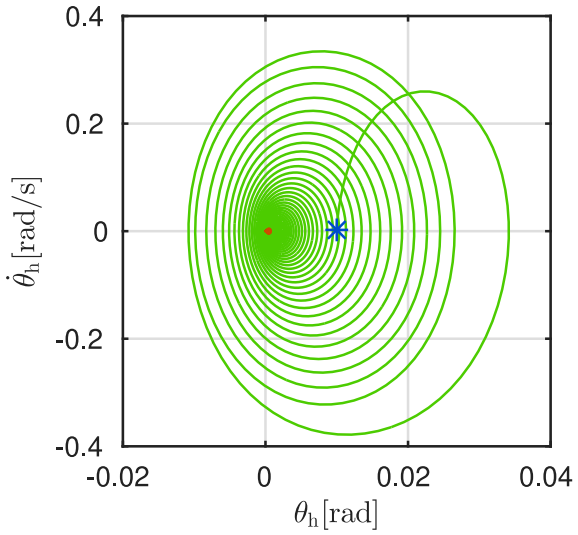

Fig. 5.6: Phase portrait of θ_h and $\dot{\theta}_\mathrm{h}$: $t = 0\,\mathrm{s}$ (∗), $0 < t \leq 15\,\mathrm{s}$ (—), $t > 15\,\mathrm{s}$ (—).

one of the most commonly used in the industry, most controllers are designed in an open-loop fashion, and they lack a formal mathematical analysis. This

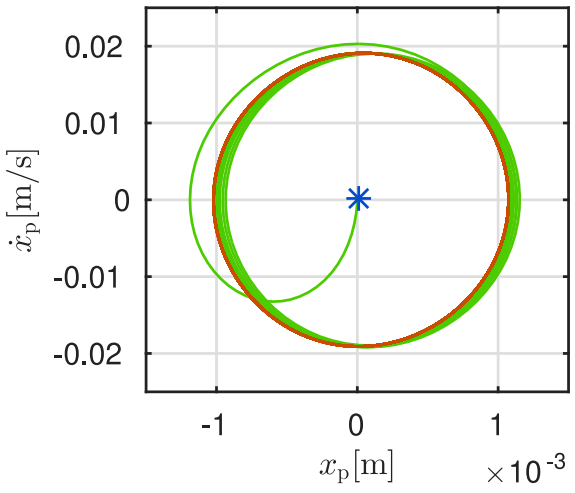

Fig. 5.7: Phase portrait of x_p and $\dot{x}_\mathrm{p}$: $t = 0\,\mathrm{s}$ (∗), $0 < t \leq 15\,\mathrm{s}$ (—), $t > 15\,\mathrm{s}$ (—).

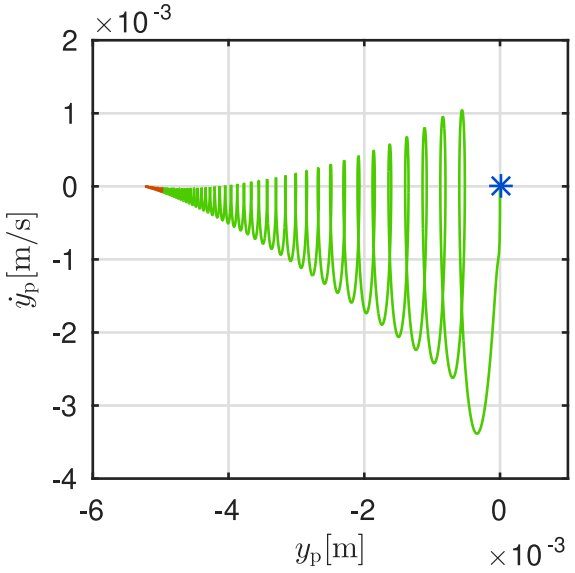

Fig. 5.8: Phase portrait of y_p and $\dot{y}_\mathrm{p}$: $t = 0\,\mathrm{s}$ (∗), $0 < t \leq 15\,\mathrm{s}$ (—), $t > 15\,\mathrm{s}$ (—).

chapter attempted to solve a particular sliding manipulation task from the model-based feedback control perspective. By employing a numerical sim-

ulation, the designed controller satisfies the desired task with the stability properties given by the mathematical analysis carried out in this chapter.

Although there are some nice features of the designed controller over the existing ones in the literature, it still has some room for improvement. In this direction, the design could be improved to obtain asymptotic stability in all the coordinates or practical asymptotic stability. The experimental evaluation of the controller is also left as remaining work. Furthermore, the generalisation of the results presented in this chapter to a more extensive set of sliding manipulation tasks is the ultimate goal pursued in this work.